Burns & Trauma, 2023, 11, tkad024
https://doi.org/10.1093/burnst/tkad024
Research Article

OXFORD

Research Article

S-Nitrosylation-mediated coupling of DJ-1 with PTEN induces PI3K/AKT/mTOR pathway-dependent keloid formation

Dongming Lv[1,†], Zhongye Xu[1,†], Pu Cheng[2,†], Zhicheng Hu[1], Yunxian Dong[3], Yanchao Rong[1], Hailin Xu[1], Zhiyong Wang[1], Xiaoling Cao[1,*] and Wuguo Deng[4,*], and Bing Tang[1,*]

[1]Department of Burn and Plastic Surgery, the First Affiliated Hospital of Sun Yat-sen University, 58 Zhongshan Road II, Guangzhou 510080, China, [2]Department of General Surgery, the Seventh Affiliated Hospital of Sun Yat-sen University, 628 Zhenyuan Road, Shenzhen, China, [3]Department of Plastic Surgery, Guangdong Second Provincial General Hospital, Southern Medical University, 466 Xingang Middle Road, Guangzhou, China and [4]Sun Yat-sen University Cancer Center, State Key Laboratory of Oncology in South China, Collaborative Innovation Center of Cancer Medicine, 651 Dongfeng East Road, Guangzhou, China

*Correspondence. tangbing@mail.sysu.edu.cn; dengwg@sysucc.org.cn; caoxiao410@sina.com

[†]Dongming Lv, Zhongye Xu and Pu Cheng contributed equally to this work.

Received 26 September 2022; Revised 15 January 2023; Accepted 3 April 2023

Abstract

Background: Keloids are aberrant dermal wound healing characterized by invasive growth, extracellular matrix deposition, cytokine overexpression and easy recurrence. Many factors have been implicated as pathological causes of keloids, particularly hyperactive inflammation, tension alignment and genetic predisposition. S-Nitrosylation (SNO), a unique form of protein modification, is associated with the local inflammatory response but its function in excessive fibrosis and keloid formation remains unknown. We aimed to discover the association between protein SNO and keloid formation.

Methods: Normal and keloid fibroblasts were isolated from collected normal skin and keloid tissues. The obtained fibroblasts were cultured in DMEM supplemented with 10% fetal bovine serum and 1% penicillin/streptomycin. The effects of DJ-1 on cell proliferation, apoptosis, migration and invasion, and on the expression of proteins were assayed. TurboID-based proximity labelling and liquid chromatography-mass spectrometry were conducted to explore the potential targets of DJ-1. Biotin-switch assays and transnitrosylation reactions were used to detect protein SNO. Quantitative data were compared by two-tailed Student's t test.

Results: We found that DJ-1 served as an essential positive modulator to facilitate keloid cell proliferation, migration and invasion. A higher S-nitrosylated DJ-1 (SNO-DJ-1) level was observed in keloids, and the effect of DJ-1 on keloids was dependent on SNO of the Cys106 residue of the DJ-1 protein. SNO-DJ-1 was found to increase the level of phosphatase and tensin homolog (PTEN) S-nitrosylated at its Cys136 residue via transnitrosylation in keloids, thus diminishing the phosphatase activity of PTEN and activating the PI3K/AKT/mTOR pathway. Furthermore, Cys106-mutant DJ-1 is refractory to SNO and abrogates DJ-1-PTEN coupling and the SNO of the PTEN protein, thus repressing the PI3K/AKT/mTOR pathway and alleviating keloid formation. Importantly,

the biological effect of DJ-1 in keloids is dependent on the SNO-DJ-1/SNO-PTEN/PI3K/AKT/mTOR axis.

Conclusions: For the first time, this study demonstrated the effect of transnitrosylation from DJ-1 to PTEN on promoting keloid formation via the PI3K/AKT/mTOR signaling pathway, suggesting that SNO of DJ-1 may be a novel therapeutic target for keloid treatment.

Key words: DJ-1, PTEN, Protein S-nitrosylation, Transnitrosylation, Keloid, S-Nitrosylation

Highlights

- SNO of the DJ-1 protein, an antioxidant and a reactive oxygen species scavenger, is an essential modulator of keloid formation.
- PTEN is found to be regulated by SNO-DJ-1, which reduces its phosphatase activity, thus mediating the activation effect of SNO-DJ-1 on the PI3K/AKT/mTOR pathway and promoting keloid formation.
- The PTEN protein is found to be S-nitrosylated via transnitrosylation from SNO-DJ-1 in keloids. The NO group is transferred from Cys106 of the DJ-1 protein to Cys136 of PTEN.

Background

Keloids, extreme aberrant dermal wound healing, are characterized by fibroblast proliferation, excessive deposition of extracellular matrix (ECM), particularly fibronectin and collagen, and cytokine overexpression [1,2]. In addition, keloids exhibit tumor-like properties that facilitate the infiltration of keloids into surrounding tissues without spontaneous regression, and usually recur after excision. Many factors have been implicated as pathological causes of keloids, particularly genetic predisposition, hyperactive inflammation and tension alignment [3–5]. However, the exact causes of keloids remain to be fully characterized.

S-Nitrosylation (SNO) is a common posttranslational protein modification that involves the modification of thiol groups of cysteine residues by nitric oxide (NO) or its derivatives [6,7]. Generally, there are two types of SNO: direct SNO of the sulfhydryl groups of cysteine, and transnitrosylation, in which a SNO intermediate is first formed, followed by transnitrosylation of the target protein. In recent years, with the development of methods to detect protein SNO [8], the physiological and pathological functions of protein SNO have been gradually revealed, such as its roles in the occurrence and development of tumors, diabetes and neurodegenerative diseases [9–11]. In addition, protein SNO is closely associated with the local inflammatory response because reactive nitrogen, which is necessary for protein SNO, is one of the products of the inflammatory response [12,13].

DJ-1, encoded by the PARK7 gene, is a 189-amino acid protein that acts as an antioxidant and a reactive oxygen species scavenger [14]. DJ-1 was initially identified as an oncogene that might be important for tumorigenesis and tumor progression [15]. It has been well established that DJ-1 is also a key pathogenic gene of early-onset Parkinson's disease, and different types of pathological deactivating mutations are common in familial early-onset Parkinson's disease [16]. Other reports have revealed that the dysregulation of DJ-1 is linked to the onset and severity of various diseases, such as obesity, ischemia–reperfusion injury, sclerosis and bone destruction [17–20]. However, to the best of our knowledge, the function of DJ-1 in chronic fibrosis of the epidermis remains unknown.

In this study, we demonstrate that DJ-1 plays a critical role in the formation of keloids. Compared to that in normal skin, the level of DJ-1 SNO is higher in keloids. DJ-1 promotes the proliferation and aggressive ability of keloid fibroblasts depending on the SNO of Cys106 in DJ-1. Further immunoprecipitation assays demonstrate that there is an interaction between DJ-1 and phosphatase and tensin homolog (PTEN), and the region in DJ-1 involved in this interaction spans amino acids 76–136. Subsequently, we confirm that DJ-1 can regulate PTEN activity through transnitrosylation, and then affect the PI3K/AKT/mTOR signaling pathway to participate in the formation of keloids. The discovery of DJ-1 as a pathogenic gene in keloids provides a potential therapeutic target to achieve a better keloid treatment outcome.

Methods

Sample collection, cell culture and reagents

Normal skin from four individuals (two men and two women, aged 15–40 years) and keloid tissues from six patients with keloids (three men and three women, aged 10–35 years, who had not received keloid treatment before surgical resection) were collected from the Department of Burns and Plastic Surgery at the First Affiliated Hospital of Sun Yat-sen University. The experiments and sample collection were performed in accordance with the Declaration of Helsinki and approved by the Research Medical Ethics Committee of the First Affiliated Hospital of Sun Yat-sen University. Informed consent was obtained from all subjects.

Keloid fibroblasts were isolated as previously described [21]. Briefly, the skin tissues were cut into small pieces and then digested with collagenase type II (S10054, Yuanye, China) at 37°C for 8 h. The fibroblasts obtained from keloid patients or from nonkeloid subjects were cultured in DMEM (Gibco, USA) supplemented with 10% fetal bovine serum and

1% penicillin/streptomycin (Thermo Fisher) in an incubator at 37°C with 5% CO_2. Cells at passages 2–5 were used for the experiments in our study. All cells were confirmed to be free of mycoplasma contamination. Neocuproine, HEPES and methyl methanethiosulfonate (MMTS) were purchased from Sigma. Biotin-HPDP and streptavidin agarose were purchased from ThermoFisher Scientific. A23187 and N^G-nitro-$_L$-arginine (NNA) were purchased from WAKO.

Plasmid construction and lentiviral transduction

First, single guide RNAs (sgRNAs) for DJ-1 were obtained from Sigma and subsequently annealed into the lentiCRISPR v2 vector to generate the DJ-1 knockout (KO) plasmids. The gRNA oligo-nucleotide sequences are as follows. DJ-1 gRNA1: sense (5′ to 3′): CACCGTAGATGTCATGAGGCGAGCT; antisense (5′ to 3′): AAACAGCTCGCCTCATGACATCTAC. DJ-1 gRNA2: sense (5′ to 3′): CACCGTGCACAGATGGCGGCTATC; antisense (5′ to 3′): AAACGATAGCCGCCATCTGTGCAC.

Second, the wild-type DJ-1 coding sequence (DJ-1-CDS) was obtained from the NCBI website and then cloned into the pSin-EF2-puro vector to generate the overexpression plasmid pSin-DJ-1. The pSin-DJ-1-V5-TurboID plasmid was constructed in a similar way.

Transfection was conducted with polyethylenimine reagent (PEI, Proteintech). To generate stable cell lines, 3×10^5 keloid fibroblasts at passage 2 were added to each well of a 6-well plate supplemented with 1 ml of DMEM, 1 ml of lentivirus and 1 : 1000 polybrene (Biosharp). After culturing at 37°C for 24 h, the medium was replaced with DMEM containing puromycin and the keloid fibroblasts were screened for 4–5 days.

Total protein extraction and western blotting

Total tissue and cell proteins were extracted using RIPA lysis buffer (Biosharp) and then centrifuged at 12,000 rpm and 4°C for 20 min. The protein concentration in the lysates was measured by the Bradford method and proteins were denatured at 100°C. Protein samples were separated and transferred as previously described [22]. After blocking with 5% nonfat milk, the membranes were incubated with primary antibodies overnight at 4°C and with horseradish peroxidase-conjugated secondary antibodies at room temperature for 1 h. High-sig ECL substrate (Tanon) was used to detect the bands with a MiniChemi chemiluminescence imager (SAGE CREATION, Beijing). The primary antibodies used were rabbit monoclonal anti-DJ1 (ab76008, Abcam), rabbit polyclonal anti-GAPDH (10494–1-AP, Proteintech), rabbit monoclonal anti-BAX (ab32503, Abcam), rabbit monoclonal anti- Bcl-xL (ab32370, Abcam), rabbit monoclonal anti-caspase-3 (ab32351, Abcam), rabbit monoclonal anti-caspase-9 (ab202068, Abcam), rabbit monoclonal anti-collagen I (ab138492, Abcam), rabbit monoclonal anti-collagen III (ab184993, Abcam), rabbit monoclonal anti-Flag tag (ab205606, Abcam), rabbit polyclonal anti-PTEN (22034–1-AP, Proteintech), rabbit polyclonal anti-phospho-AKT (28731–1-AP, Proteintech), rabbit polyclonal anti-AKT (10176–2-AP, Proteintech), mouse monoclonal anti-phospho-mTOR (67778–1-Ig, Proteintech) and mouse monoclonal anti-mTOR (66888–1-Ig, Proteintech).

In vitro cell proliferation, migration and invasion assays

Stable keloid fibroblasts were seeded in 96-well microplates at a density of 2000 cells per well, and a cell counting kit-8 (CCK-8) assay was conducted according to the manufacturer's instructions to measure cell viability.

For cell migration and invasion assays, the experimental procedure was carried out as previously described [23].

Apoptosis assay by flow cytometry

Stable keloid fibroblasts were suspended and washed twice with PBS. An Annexin V PE/7-AAD apoptosis detection kit (4A Biotech) was used to treat the collected cells according to the manufacturer's instructions, and the stained cells were analysed with a Gallios flow cytometer (Beckman Coulter).

In vivo experiment

Animal experiments were approved by the Animal Research Committee of the First Affiliated Hospital of Sun Yat-sen University and were executed according to established guidelines for laboratory animals. Nude mice, 4–5 weeks old, were purchased from GemPharmatech (Nanjing, China). Keloid tissues were collected from four patients diagnosed with keloids and without any chronic diseases (three men and one woman, aged 19–35 years). Keloid tissues with a size of $6 \times 5 \times 4$ mm were subcutaneously transplanted into the scapular area of the nude mice. All mice survived without rejection responses. To knockdown DJ-1, 5 nmol siRNA was dissolved in 50 μl of saline buffer and subsequently injected into the keloid tissues with a microsyringe every 3 days. Tissue size measurements were taken every 3 days. After 5 weeks, the xenograft tissues were harvested, photographed and fixed with formalin. Tissue sizes were measured with the following formula: $\text{width}^2 \times \text{length} \times \pi/6$. The researchers remained blinded to the group allocation during the outcome assessment.

Immunohistochemistry assay

The harvested keloid tissue slides were deparaffinized and rehydrated followed by antigen retrieval. The keloid tissues were blocked with 5% normal goat serum with 0.1% Triton X-100 and 3% H_2O_2 in PBS, and then incubated with antibodies against Ki-67 (1 : 500, ab15580, Abcam) and α-SMA (1 : 500, CST, 19245 T) overnight at 4°C. The staining continued with horseradish peroxidase conjugates using 3,3′-diaminobenzidine (DAB) detection. The levels of IHC staining were then evaluated by two independent pathologists. The sections were captured using a microscope (EVOS FL Auto Cell Imaging System).

TurboID-based proximity labelling and liquid chromatography-mass spectrometry

Keloid fibroblasts overexpressing DJ-1-V5-TurboID were treated with 50 μM biotin for 30 min. The protein was extracted using RIPA lysis buffer and then treated with ultrasound for 3 min. After centrifugation, part of the protein supernatant was denatured for the detection of whole-cell lysis and the other part was incubated with streptavidin beads (Cytiva) at 4°C overnight. Then, the beads were washed using 1 ml of RIPA lysis buffer, 1 ml of KCl, 1 ml of Na_2CO_3, 1 ml of 2 M urea (pH 8.0) and 1 ml of RIPA lysis buffer in sequence. Then, 100 μl of elution buffer was added to the beads and heated for 10 min at 95°C. The beads were separated magnetically and elution buffer containing biotinylated proteins was collected for further mass spectrometric analysis. In the liquid chromatography-mass spectrometry (LC–MS) experiment, after reduction and alkylation, the samples were treated with trypsin (mass ratio 1 : 50) and digested at 37°C for 20 h. After desalting, the digested product was lyophilized, redissolved in a 0.1% FA solution and stored at −20°C until further use. The mass/charge ratios of the peptides and peptide fragments were obtained as follows: 20 fragment profiles were collected after each full scan. The raw file was searched by Proteome Discoverer1.4 software and the identified protein results were obtained.

Biotin-switch assay to detect protein SNO

For the biotin-switch assay, keloid tissues or cells were lysed in HENS buffer (100 mM HEPES, 0.1% SDS, 0.1 mM neocuproine, 1 mM EDTA, 1% Triton X-100, pH 7.4). Free cysteine residues were blocked with MMTS. More specifically, 1 mg of each protein sample was diluted to 1.8 ml with HEN buffer (100 mM HEPES, 1 mM EDTA, 0.1 mM neocuproine, pH 8.0) [24]. Next, 0.2 ml of 25% SDS was added, along with 20 μl of 10% MMTS (to reach a final volume of 2 ml and final concentrations of 2.5% SDS and 0.1% MMTS); the mixture was incubated at 50°C in the dark for 20 min with frequent vortexing. Three volumes of cold acetone were added to each sample. Proteins were precipitated for 20 min at −20°C and collected by centrifugation at 2000 × g for 5 min. The supernatant was discarded and the protein pellets were gently washed with 70% acetone at 4°C. Proteins were resuspended in 0.24 ml of HENS buffer and transferred to a fresh 1.7 ml microfuge tube containing 30 μl of biotin-HPDP (1 mM) with or without sodium ascorbate (20 mM) [25]. The sample was incubated in the dark at room temperature for 1 h. Three volumes of cold acetone were added to each sample (0.9 ml). Proteins were precipitated for 20 min at −20°C and collected by centrifugation at 5000 × g for 5 min. The supernatant was discarded and the protein pellets were gently washed with 70% acetone at 4°C. After resuspension with 0.25 ml of HENS buffer, 0.75 ml of neutralization buffer was added. A small portion of each sample (∼10 μl) was used to analyse the protein composition. The remaining samples were transferred to new 1.5 ml microfuge tubes and 30 μl of streptavidin agarose beads was added. Immunoprecipitated proteins were extracted from the beads by boiling in sample buffer, separated by SDS-PAGE, transferred to PVDF membranes and then incubated with antibodies.

PTEN phosphatase assay

The phosphatase activity of PTEN was measured with a malachite green phosphatase assay kit (AmyJet Scientific Inc) according to the manufacturer's protocol. Standard curves were plotted with phosphate standard protein. Subsequently, the protein was incubated with malachite green solution and the released phosphate was quantified by reading the absorbance at 620 nm. To test intracellular PTEN activity, the cells were first lysed in lysis buffer. Immunoprecipitation was then performed using anti-PTEN antibodies and protein A/G agarose beads. Then, the phosphatase activity of the PTEN protein was determined by the malachite green phosphatase method.

Recombinant proteins and transnitrosylation reactions

pSKB-His-PTEN and pSKB-His-DJ-1 were purchased from Guangzhou Geidan Biological Technology (China Guangzhou). Protein production was induced with 1 mM isopropyl-beta-D-thiogalactoside. For the transnitrosylation assays, recombinant PTEN (0.2 μM) or DJ-1 (2 μM) prepared from bacteria was incubated with 25 μM S-nitrosocysteine (SNOC) for 40 min at room temperature in the dark. Subsequently, each of the resulting S-nitrosylated proteins was used as a potential NO donor for the non-nitrosylated form of the other protein in a 40-min reaction at room temperature in the dark to detect potential transnitrosylation. The resulting samples were subjected to the biotin-switch assay to monitor the SNO status of each protein.

Collagen gel contraction assay

Keloid fibroblasts (6×10^5 cells/ml, 2 ml) were mixed with rat tail collagen (Solarbio, 5 mg/ml, 900 μl) and 10 × DMEM (100 μl) and then cultured in 24-well plates at 37°C for 30 min. The generated collagen gels were taken out for photography 24 or 48 h later. The difference in gel area was calculated.

Statistical analysis

Statistical analysis and mapping were performed by SPSS 25.0 or GraphPad Prism 8.0. The data are presented as the mean ± standard deviation. Each experiment was independently conducted three times. When comparing two groups, quantitative data were compared by two-tailed Student's *t* test. One-way ANOVA with Tukey's multiple comparisons test was used for more than two groups with a single variable, and two-way ANOVA with Tukey's multiple comparisons test

was used for experimental set-ups with a second variable. A p value < 0.05 was considered to indicate statistical significance.

Results

DJ-1 is an essential modulator of keloid formation

Because the function of DJ-1 in chronic fibrosis of the epidermis is unknown, to investigate the effect of DJ-1 on keloid formation, we established stable DJ-1 KO keloid fibroblasts by using two specific sgRNAs against DJ-1 (referred to as DJ-1 sg1 and sg2; Figure 1a). Cell proliferation assays showed that the suppression of DJ-1 expression by CRISPR/Cas9-based KO significantly reduced the viability of keloid fibroblasts (Figure 1b). In addition, a cell apoptosis assay performed by flow cytometry suggested that the loss of DJ-1 markedly enhanced the apoptosis rate of keloid fibroblasts (Figure 1c). We then determined the protein expression of apoptosis-related molecules such as BAX, Bcl-xL, caspase 3 and caspase 9, and in line with the apoptosis assay results, we observed increased expression of the proapoptotic proteins BAX, caspase 3 and caspase 9 but downregulated expression of the antiapoptotic protein Bcl-xL due to DJ-1 KO (Figure 1d). Additionally, we monitored the effect of DJ-1 on the migration and invasion of keloid fibroblasts and observed decreased migration and invasion in DJ-1-KO cells (Figure 1e). Furthermore, the expression levels of collagen I and collagen III were decreased in DJ-1-KO cells (Figure 1f).

There are several mutations in DJ-1 that are associated with autosomal recessive early-onset parkinsonism [26], and these mutations have also been observed in tumors. Thus, we wondered whether these mutations in DJ-1 are responsible for its effect on keloid formation. Therefore, we first constructed a flag-tagged wild-type (WT) DJ-1 plasmid and plasmids containing the sequences of other disease-associated DJ-1 mutants (M26I, E64D, R98Q, A104T, D149A, G150S, E163K, L166P and A171S; https://www.uniprot.org/) and established the corresponding stable cell lines (Figure 1g). DJ-1-overexpressing cells exhibited greater cell proliferation, and to our surprise, the other cells expressing mutant DJ-1 had a similar capacity (Figure 1h). Subsequently, we monitored cell migration and invasion under the same conditions. The overexpression of not only WT DJ-1 but also the DJ-1 mutants obviously enhanced cell migration and invasion (Figure 1i). These results suggest that the key role of DJ-1 in keloid formation is attributable to a specific modification at the gene or protein level.

We subsequently determined the role of DJ-1 in keloids *in vivo*. Knockdown of DJ-1 significantly reduced the volume of keloid tissues in the nude mice (Figure 1j). Hematoxylin and eosin staining showed a smaller number of collagen fibers in DJ-1 knockdown groups. In addition, immunohistochemistry staining of keloid tissues showed that proliferation- and fibrosis-related gene expression (such as Ki-67 and α-SMA) was reduced in the DJ-1 knockdown groups (Figure 1k). These data suggest the essential role of DJ-1 in modulating keloid formation.

SNO of DJ-1 is responsible for its effect on keloids

An increasing number of studies have demonstrated that protein SNO contributes greatly to chronic inflammatory diseases [27,28]. As keloids are known to be associated with continuous local inflammation, protein SNO may play a critical role in keloid formation. Since certain modifications are associated with the function of DJ-1 in keloids, we wondered whether protein SNO plays an important role in the function of DJ-1. First, we monitored the expression of DJ-1 as well as its SNO in normal fibroblasts and keloid fibroblasts. Interestingly, we observed no difference in the total DJ-1 protein level between the cells. However, the level of DJ-1 SNO was found to be higher in keloid fibroblasts than in normal fibroblasts (Figure 2a). Then we further confirmed this observation in normal skin and keloid tissue and observed similar results (Figure 2b). To assess S-nitrosylated DJ-1 (SNO-DJ-1) formation, we detected the level of SNO-DJ-1 in keloid fibroblasts treated with the physiological NO donor SNOC. The level of SNO-DJ-1 was positively correlated with the concentration of SNOC (Figure 2c). Nitric oxide synthase (nNOS) is a key enzyme in NO synthesis. To investigate whether the activation of nNOS to generate endogenous NO could S-nitrosylate DJ-1, we exposed keloid fibroblasts to the calcium ionophore A23187 to activate nNOS. Under these conditions, we found by biotin-switch assays that A23187 treatment increased the SNO-DJ-1 levels; moreover, the NOS inhibitor NNA blocked this reaction (Figure 2d). SNO occurs at the cysteine residues of proteins, and DJ-1 contains three potential redox-active cysteine residues (Cys46, Cys53 and Cys106). We next mutated the active-site cysteine and exogenously expressed the WT and mutant DJ-1 proteins in endogenous DJ-1-KO keloid fibroblasts. A lower SNO-DJ-1 level was observed when DJ-1 with a mutation at Cys106 was exogenously expressed, which indicated that SNO of the DJ-1 protein mainly occurs at Cys106 (Figure 2e).

To explore whether the SNO of Cys106 was responsible for the effect of DJ-1 on keloids, we exogenously expressed WT DJ-1 and the C106A mutant in keloid fibroblasts (Figure 2f). Cell proliferation was dramatically enhanced in the WT DJ-1 group, whereas there was no difference when the C106A mutant was overexpressed (Figure 2g). A similar phenomenon was observed when cell migration and invasion were measured (Figure 2h). Additionally, exogenous expression of the C106A mutant did not increase the levels of collagen I and collagen III, as observed with WT DJ-1 (Figure 2i). Collectively, our results demonstrated that the SNO of DJ-1 at Cys106 is responsible for its effect on keloids.

Identification of potential DJ-1 targets using TurboID-based proximity labelling

To identify potential targets of DJ-1, we employed TurboID-based proximity labelling combined with LC–MS to identify

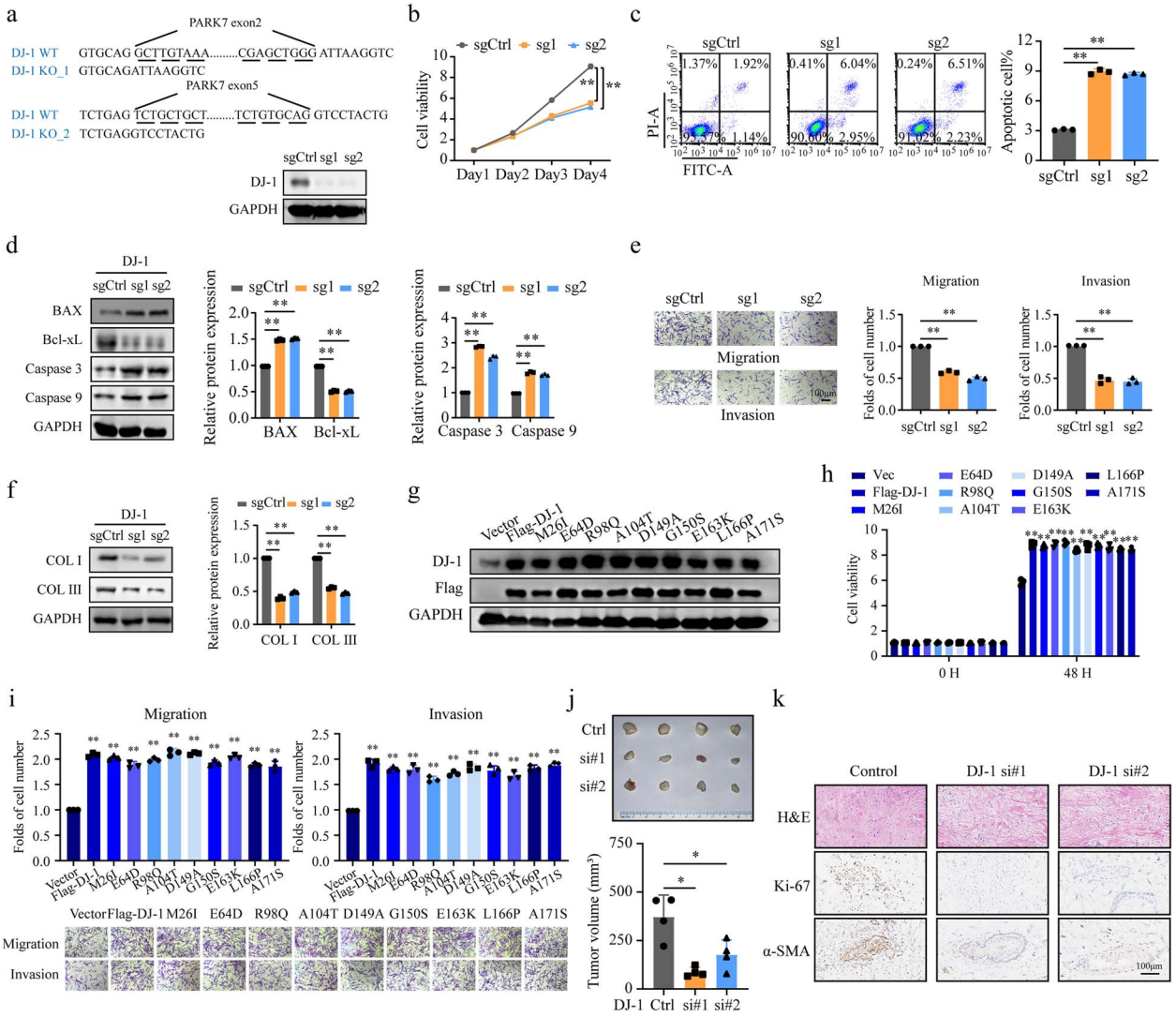

Figure 1. DJ-1 is an essential modulator of keloid formation. (**a**) The results of sequencing and Western blot analysis of DJ-1 expression in keloid fibroblasts mediated by CRISPR/Cas9. (**b**, **c**) Cell proliferation and apoptosis of DJ-1-KO keloid fibroblasts. (**d**) Western blot analysis of BAX, Bcl-xL, caspase 3 and caspase 9 expression in the indicated cells. (**e**) Cell migration and invasion of the indicated cells. Scale bar: 20μm. (**f**) Western blot analysis of collagen (COL) I and COL III expression in the indicated cells. (**g**) Verification of the overexpression of wild type (WT) DJ-1 and DJ-1 mutants in keloid fibroblasts. (**h**, **i**) Cell proliferation, migration and invasion of the indicated cells. (**j**) Vlume and general view of keloid tissues in nude mice treated with or without knockdown of DJ-1 (n = 4). (**k**) Hematoxylin and eosin stain, Ki-67 staining and α-SMA staining of keloid tissues from nude mice. Scale bar: 100 μm; $^{*}p < 0.05$, $^{**}p < 0.01$. *DJ-1* parkinson disease protein 7, *PARK7* parkinson disease 7, *BAX* BCL2-Associated X, *Bcl-xL* BCL2-like 1, *COL* collagen I

cellular proteins that can directly bind DJ-1 [29,30]. We transfected DJ-1-V5-TurboID plasmids into keloid fibroblasts, as shown in Figure 3a. Biotin (50 μM) was added to the culture medium for labelling 10 min before lysis. Streptavidin beads were used to capture biotinylated proteins from the lysates, which was followed by LC–MS analysis. Previous studies have shown that the PI3K/AKT/mTOR pathway plays an important role in the occurrence and development of keloids. Among the potential DJ-1-binding proteins identified from our MS data, several regulators of the PI3K/AKT/mTOR pathway attracted our attention, including PTEN, RPTOR, RHEB and AKT (Figure 3b). Among them, PTEN, an essential negative modulator of this pathway, was enriched in most fragments (Figure 3c). Immunoprecipitation assays verified that DJ-1 could directly bind PTEN in keloid fibroblasts (Figure 3d, e). Additionally, we observed that DJ-1 was located in the cytoplasm and nucleus in keloid fibroblasts and colocalized with PTEN (Figure 3f). To further determine the regions of DJ-1 that interact with PTEN, a series of DJ-1 fragments was generated, as illustrated in Figure 3g, and their interaction with PTEN was tested. We found that the binding of DJ-1 with PTEN was completely abolished when the region consisting of residues 76–136 was absent, which was consistent with the above finding about the SNO of DJ-1 at Cys106. Taken together, these results suggest that PTEN is a potential interaction target of DJ-1 that may mediate the regulatory effect of DJ-1 on the PI3K/AKT/mTOR pathway.

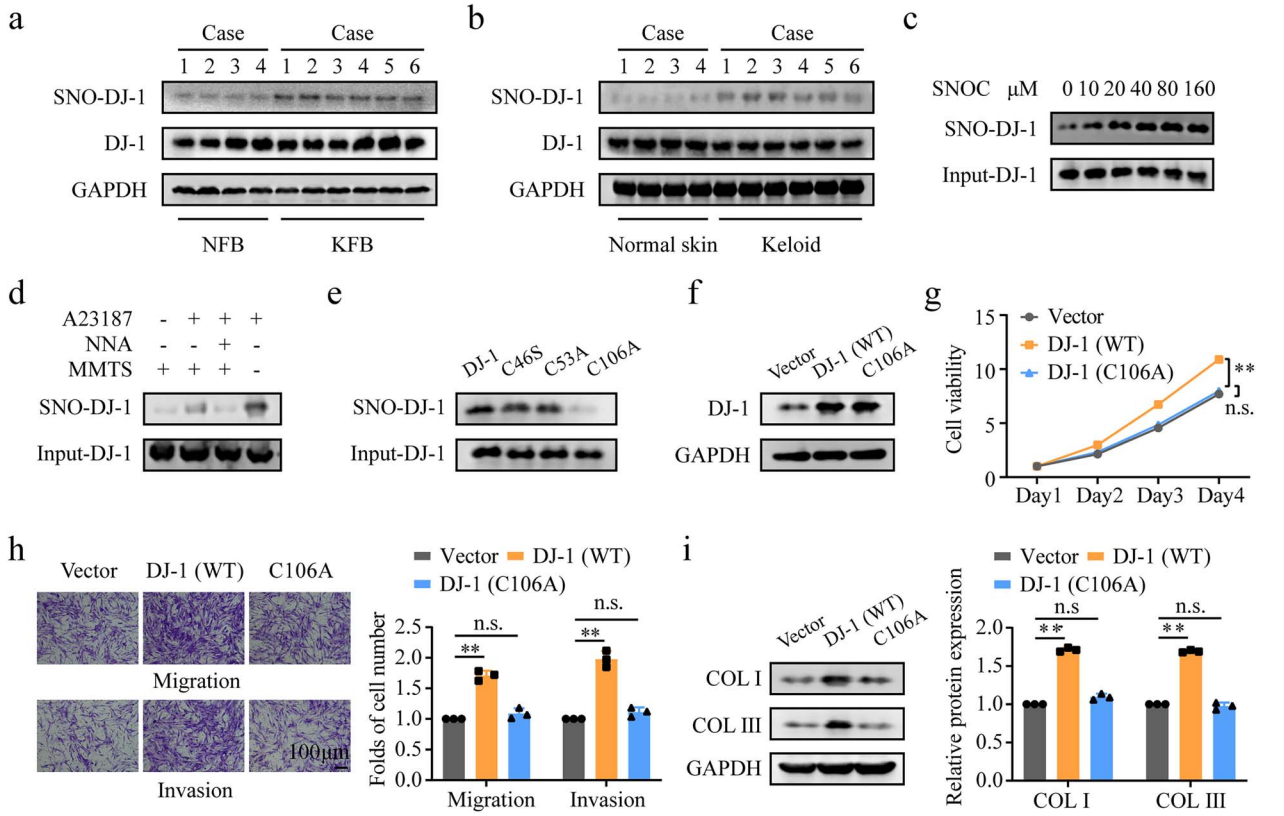

Figure 2. S-Nitrosylation of DJ-1 is responsible for its effect on keloids. (**a**, **b**) Western blot analysis of SNO-DJ-1 and DJ-1 expression in the indicated fibroblasts and skin tissues. (**c**) Western blot analysis of SNO-DJ-1 and DJ-1 expression in keloid fibroblasts treated with the NO donor SNOC. (**d**) SNO-DJ-1 and DJ-1 expression in keloid fibroblasts treated with the calcium ionophore A23187, the NOS inhibitor N^G-nitro-$_L$-arginine (NNA) and methyl methanethiosulfonate (MMTS). MMTS was used to block free sulfhydryl groups in S-nitrosylated proteins. (**e**) SNO-DJ-1 and DJ-1 expression in endogenous DJ-1-KO keloid fibroblasts exogenously expressing WT or mutant DJ-1. (**f**) Verification of the overexpression of WT DJ-1 and the DJ-1-C106A mutant in keloid fibroblasts. (**g**, **h**) Cell proliferation, migration and invasion of the indicated cells. Scale bar: 100 μm. (**i**) Western blot analysis of collagen (COL) I and COL III generation in the indicated cells. $^{**}p < 0.01$, n.s., not significant. *DJ-1* parkinson disease protein 7, *SNO* S-nitrosylation, *SNOC* S-nitrosocysteine, *NFB* normal fibroblasts, *KFB* keloid fibroblasts, *MMTS* methyl methanethiosulfonate, *NNA* NG-nitro-L-arginine, *WT* wild type, *COL* collagen

S-Nitrosylated PTEN is more abundant in keloids and is transnitrosylated from SNO-DJ-1

Since the level of SNO-DJ-1 was higher in keloids and PTEN was proven to be a potential interaction target of DJ-1, we wondered whether PTEN would also be S-nitrosylated in keloids. We first measured the level of S-nitrosylated PTEN (SNO-PTEN) in normal fibroblasts and keloid fibroblasts. Similar to the results for DJ-1, we found a higher SNO-PTEN level in keloid fibroblasts than in normal fibroblasts (Figure 4a). In addition, a higher level of SNO-PTEN was observed in keloid tissue (Figure 4b). To assess SNO-PTEN formation, we detected the level of SNO-PTEN in keloid fibroblasts treated with the physiological NO donor SNOC. The SNO-PTEN level was positively correlated with the concentration of SNOC (Figure 4c). Subsequently, we exposed keloid fibroblasts to the calcium ionophore A23187 to activate nNOS. After that, we found by the biotin-switch assay that endogenous NO increased the level of SNO-PTEN; moreover, the NOS inhibitor NNA blocked this effect (Figure 4d). These results demonstrated that SNO-PTEN was present at higher levels in keloids, and this SNO may be generated by direct SNO from an NO donor or through transnitrosylation.

To further elucidate the mechanism of SNO-PTEN formation, we next incubated the purified recombinant DJ-1 protein with the NO donor SNOC to generate the SNO-DJ-1 protein *in vitro* and subsequently mixed SNO-DJ-1 or unmodified DJ-1 with PTEN to monitor potential transnitrosylation. We found by a biotin-switch assay that PTEN was S-nitrosylated when mixed with SNO-DJ-1 but not unmodified DJ-1, suggesting that SNO-DJ-1 could act as an NO donor. In contrast, purified recombinant SNO-PTEN protein was generated in the same way but could not transfer NO to the DJ-1 protein (Figure 4e). These results demonstrated that NO could be transferred from DJ-1 to PTEN but not vice versa. Furthermore, we exogenously expressed the C46S, C53A and C106A DJ-1 mutants in DJ-1-KO keloid fibroblasts and concurrently incubated them with the NO donor SNOC. Surprisingly, we did not observe the generation of SNO-PTEN when the C106A DJ-1 mutant was overexpressed, even in the presence of SNOC (Figure 4f). In addition, MS analysis showed that Cys136 was the residue on the PTEN protein

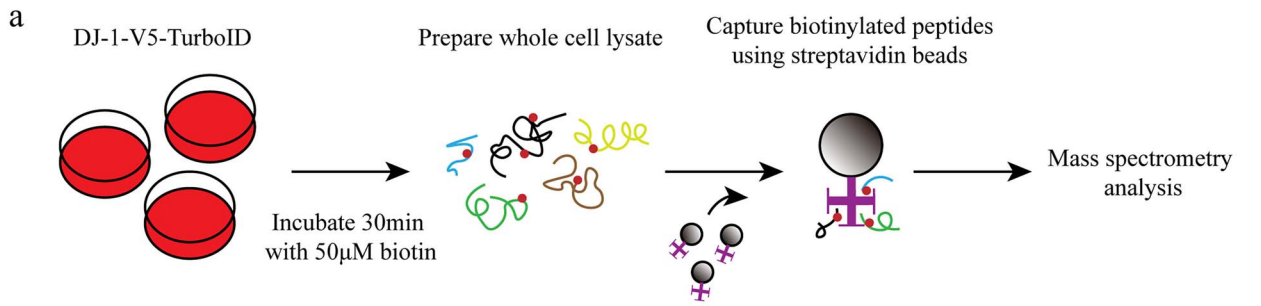

b

Unique	Total	Gene
14	14	DJ-1
14	14	PTEN
6	6	RPTOR
5	5	RHEB
1	1	AKT

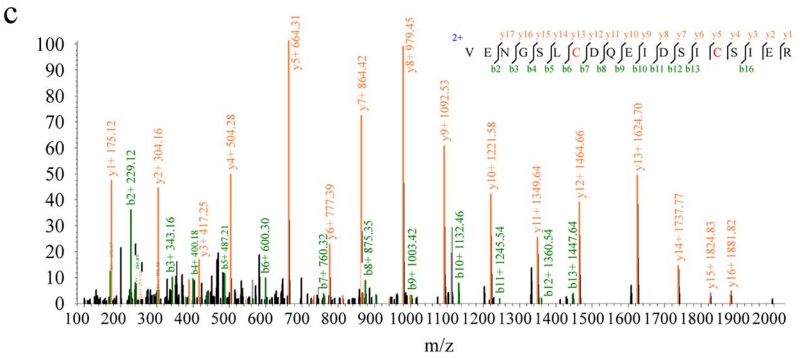

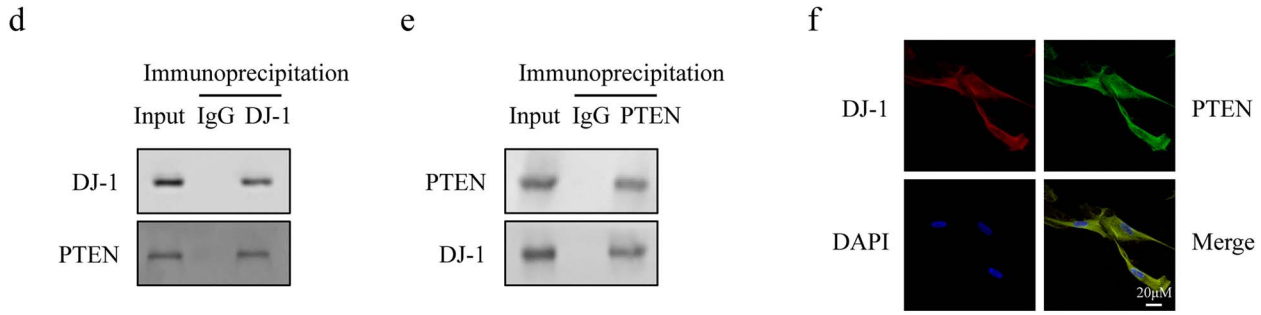

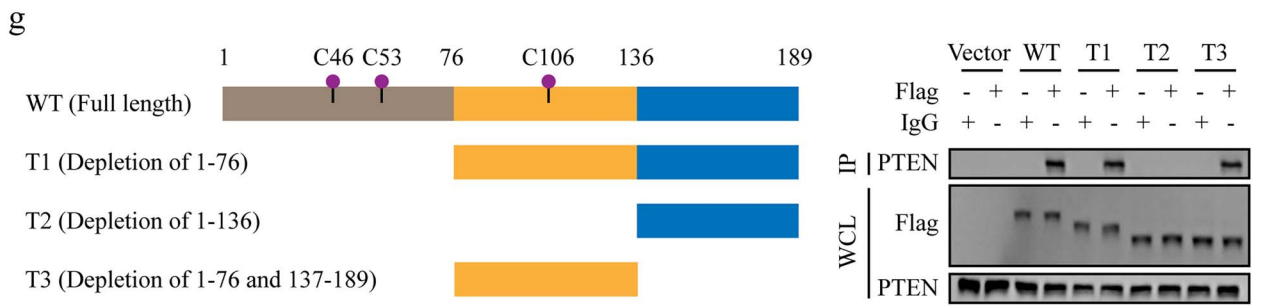

Figure 3. Identification of potential DJ-1 targets using TurboID-based proximity labelling. (**a**) Schematic diagram depicting the process used to identify the potential targets of DJ-1. (**b**) A partial list of proteins identified from mass spectrometic analysis of cells stably expressing DJ-1-V5-TurboID. The numbers of unique and total peptides corresponding to the indicated proteins are shown. (**c**) Mass spectrum analysis showing the PTEN protein. (**d, e**) Immunoprecipitation of DJ-1 and PTEN. (**f**) Immunofluorescent staining showing the cellular locations of DJ-1 and PTEN. Scale bar: 20 μm. (**g**) Schematic illustration of DJ-1 mutants in which the indicated regions were depleted and western blot analysis by immunoprecipitation using flag-agarose. *DJ-1* parkinson disease protein 7, *PTEN* phosphatase and tensin homolog, *RPTOR* regulatory associated protein of MTOR complex 1,*AKT* Akt kinase, *WCL* whole cell lysis, *IP* immunoprecipitation

that underwent transnitrosylation (Figure 4g). In general, SNO-PTEN generation can be ascribed to transnitrosylation from SNO-DJ-1 but not to direct SNO from an NO donor.

SNO-PTEN mediates the effect of DJ-1 on the PI3K/AKT/mTOR pathway

Since PTEN has specific phosphatase activity and can participate in cell regulation through dephosphorylation, we wondered whether SNO would affect its activity. First, we measured PTEN activity in keloid fibroblasts and normal fibroblasts. Decreased PTEN activity was observed in keloid fibroblasts (Figure 5a). To explore whether the SNO of PTEN could contribute to its decreased activity, we treated keloid fibroblasts with increasing concentrations of the NO donor SNOC and found that the phosphatase activity decreased with increasing SNOC concentration (Figure 5b). Moreover,

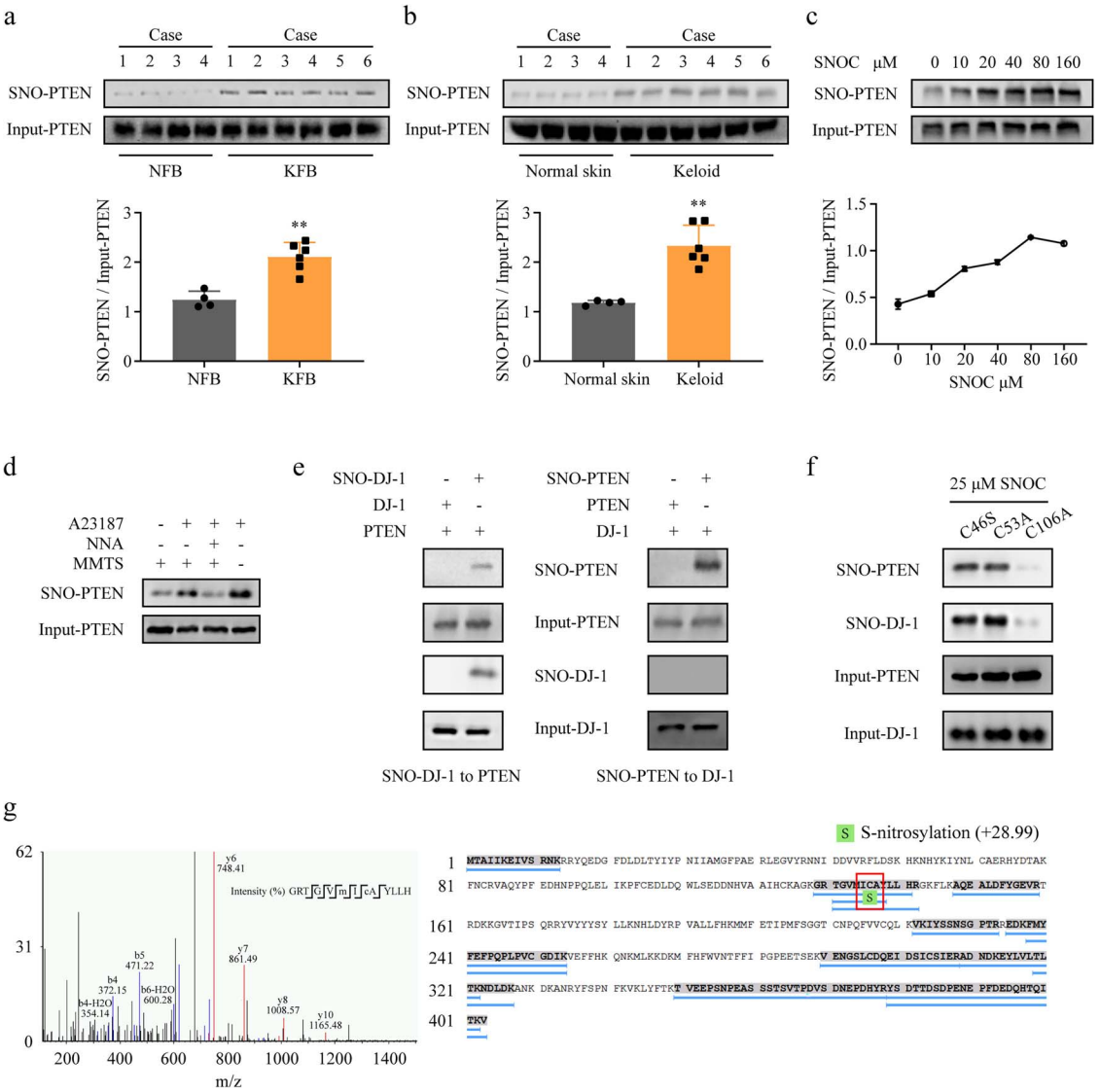

Figure 4. SNO-PTEN is more abundant in keloids and is formed by transnitrosylation from SNO-DJ-1. (**a**, **b**) Western blot analysis of SNO-PTEN and PTEN expression in the indicated fibroblasts and skin tissues. (**c**) SNO-PTEN and PTEN expression in keloid fibroblasts treated with the NO donor SNOC. (**d**) SNO-PTEN and PTEN expression in keloid fibroblasts treated with the calcium ionophore A23187, the NOS inhibitor N^G-nitro-$_L$-arginine (NNA) and methyl methanethiosulfonate (MMTS). (**e**) A nitrosylation assay with the DJ-1 and PTEN proteins was conducted. (**f**) SNO-DJ-1, DJ-1, SNO-PTEN and PTEN expression in endogenous DJ-1-KO keloid fibroblasts exogenously expressing DJ-1 mutants. (**g**) Mass spectrum showing the transnitrosylation site of the PTEN protein. $^{**}p < 0.01$. *DJ-1* parkinson disease protein 7, *PTEN* phosphatase and tensin homolog, *SNO* S-nitrosylation, *SNOC* S-nitrosocysteine, *NFB* normal fibroblasts, *KFB* keloid fibroblasts, *MMTS* methyl methanethiosulfonate, *NNA* NG-nitro-L-arginine

we exposed keloid fibroblasts to the calcium ionophore A23187 with or without the NOS inhibitor NNA. The phosphatase activity of PTEN was significantly diminished after A23187 treatment, but this effect was reversed by NNA (Figure 5c).

Subsequently, we further explored how SNO-PTEN coordinates the relationship between DJ-1 and signaling pathways. We initially measured the PI3K/AKT/mTOR pathway in keloids and found that the p-AKT/AKT and p-mTOR/mTOR ratios were increased in keloid fibroblasts and keloid tissues (Figure 5d, e). We next treated keloid fibroblasts with the NO donor SNOC to generate high levels of SNO-DJ-1 and SNO-PTEN; notably, the PI3K/AKT/mTOR pathway was further activated under these conditions (Figure 5f). In addition, the p-AKT/AKT and p-mTOR/mTOR ratios were reduced in DJ-1-KO keloid fibroblasts and upregulated in WT DJ-1-overexpressing cells but not in C106A mutant DJ-1-overexpressing cells (Figure 5g, h). Additionally, we treated keloid fibroblasts with the PI3K inhibitor wortmannin and incubated them with the NO donor SNOC. Thus, we observed that the upregulation of p-AKT due to the SNO of PTEN by exogenous NO could be diminished by wortmannin treatment, suggesting that SNO-PTEN activates the AKT signaling pathway through PI3K (Figure 5i). Given these findings, we conclude that SNO-PTEN can mediate the activating effect of DJ-1 on the PI3K/AKT/mTOR pathway.

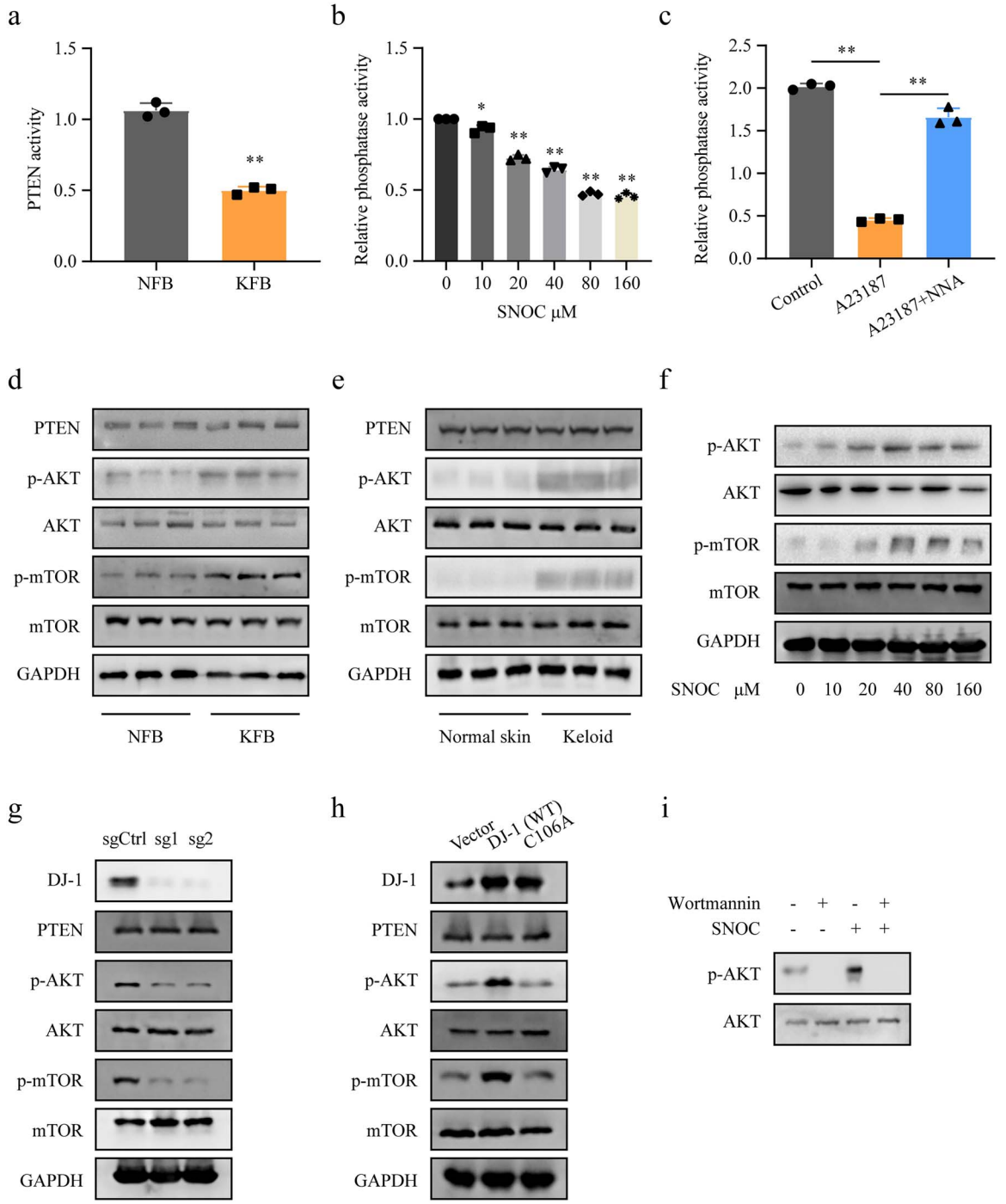

Figure 5. SNO-PTEN mediates the effect of DJ-1 on the PI3K/AKT/mTOR pathway. (**a**) Measurement of PTEN activity in normal fibroblasts and keloid fibroblasts. (**b**) Relative phosphatase activity in keloid fibroblasts treated with increasing concentrations of the NO donor SNOC. (**c**) Relative phosphatase activity in keloid fibroblasts treated with A23187 and NNA. (**d**, **e**) Western blot analysis of the PI3K/AKT/mTOR pathway in the indicated fibroblasts and skin tissues. (**f**) Western blot analysis of the PI3K/AKT/mTOR pathway in keloid fibroblasts treated with increasing concentrations of SNOC. (**g**, **h**) Western blot analysis of the PI3K/AKT/mTOR pathway in DJ-1-KO and DJ-1-overexpressing keloid fibroblasts. (**i**) Western blot analysis of p-AKT and AKT expression in keloid fibroblasts treated with the PI3K inhibitor wortmannin. $^{*}p < 0.05$, $^{**}p < 0.01$. *DJ-1* parkinson disease protein 7, *PTEN* phosphatase and tensin homolog, *AKT* Akt kinase, *mTOR* mechanistic target of rapamycin kinase, *SNOC* S-nitrosocysteine, *NFB* normal fibroblasts, *KFB* keloid fibroblasts

DJ-1 promotes keloid formation via the PI3K/AKT/mTOR pathway

Since DJ-1 was proven to be an essential modulator of keloid formation and SNO-DJ-1 could regulate the PI3K/AKT/mTOR pathway through transnitrosylation to PTEN, we asked whether the effect of DJ-1 on keloid formation depends on the PI3K/AKT/mTOR pathway. To address this question, we constructed stable WT

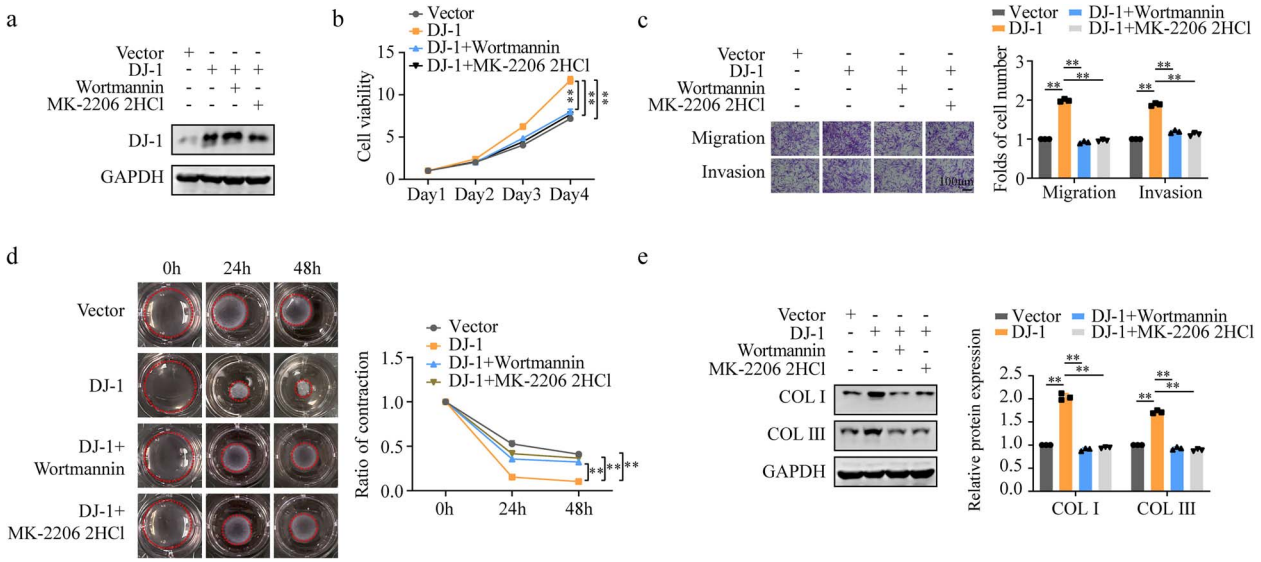

Figure 6. DJ-1 promotes keloid formation via the PI3K/AKT/mTOR pathway. (**a**) Verification of DJ-1 expression in DJ-1-overexpressing cells treated with the PI3K inhibitor wortmannin and the AKT inhibitor MK-2206 2HCl. (**b, c**) Proliferation, migration and invasion of the indicated cells. Scale bar: 100 μm. (**d**) Collagen (COL) gel contraction assay conducted in the indicated cells. (**e**) Measurement of COL I and COL III generation in the indicated cells by Western blotting. $^{**}p < 0.01$. *DJ-1* parkinson disease protein 7, *COL* collagen

DJ-1-expressing keloid fibroblasts and treated them with the PI3K inhibitor wortmannin or the AKT inhibitor MK-2206 2HCl (Figure 6a). We observed that when cell viability was increased by WT DJ-1 overexpression, this increase could be antagonized by wortmannin or MK-2206 2HCl treatment (Figure 6b). We then measured the migration and invasion of these cells and found that wortmannin and MK-2206 2HCl could also block the stimulatory effect generated by DJ-1 (Figure 6c). In addition, we mixed the WT DJ-1-overexpressing keloid fibroblasts with rat tail collagen. After 48 h, the collagen in the DJ-1-overexpressing group was significantly more contracted than that in the control group, whereas this effect was diminished by wortmannin and MK-2206 2HCl (Figure 6d). The increases in collagen I and collagen III levels upon DJ-1 overexpression could be reversed by wortmannin and MK-2206 2HCl (Figure 6e). In conclusion, we found that DJ-1 promotes keloid formation in a manner dependent on the PI3K/AKT/mTOR pathway.

Discussion

Excessive proliferation of fibroblasts and invasion towards peripheral healthy skin are the hallmarks of keloids, which are thought to be closely associated with persistent local inflammation. In response to inflammation, many cell types involved in immunity and inflammation produce large amounts of NO. Accumulating studies have revealed that NO production is increased in keloid scar tissues compared with perilesional skin tissues, and exogenous NO participates in keloid formation [31–33]. Protein SNO is a typical redox-dependent posttranslational protein modification, which is a nonenzymatic reversible process and mainly depends on the proximity of proteins to diffuse NO [7]. Protein SNO has attracted increasing attention in recent years due to its complexity and the involvement of multiple pathways, which has further provided new perspectives for the clinical treatment of various diseases, such as atherosclerosis, neurodegenerative disorders, tumors and diabetes [10,28,34,35]. Given this, protein SNO may be involved in the pathology of continuous expansion in keloids. However, to date, the relationship between protein SNO and keloid formation has not been reported.

DJ-1, an antioxidant and a reactive oxygen species scavenger, is a promising therapeutic candidate for various diseases, such as neurodegenerative diseases, ischemia–reperfusion injury and cancer. Additionally, DJ-1 has been reported to be involved in immune and inflammatory regulation, mainly by coordinating the activation of several immune cells, including mast cells, T cells and macrophages, via ROS-dependent or ROS-independent mechanisms [36]. However, the function and mechanism of DJ-1 in keloid formation are still unclear. In this study, we found that DJ-1, an essential modulator of keloids, promoted cell viability, migration and invasion, and collagen generation in keloid fibroblasts. Surprisingly, the DJ-1 protein was S-nitrosylated and the SNO-DJ-1 level was higher in keloid tissue than in normal skin. The biological effect of DJ-1 on keloid formation was dependent on protein SNO at the Cys106 residue. We present the first study to suggest that DJ-1 could be a novel therapeutic candidate for keloids, and the results further reflect the important role of protein SNO in keloid formation.

PTEN, a gene located on chromosome 10, encodes a protein composed of 403 amino acids with phosphatase activity. PTEN is known as a negative regulator of the PI3K/AKT/mTOR pathway by promoting the dephosphorylation of PI-3,4,5-P3 to PI-P2 and inhibiting the activation of downstream AKT. PTEN dysfunction can lead

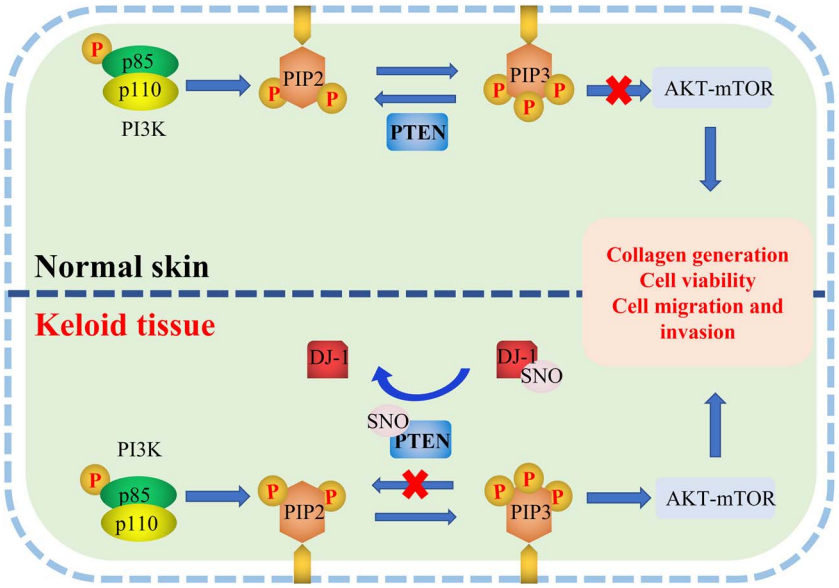

Figure 7. Schematic diagram showing transnitrosylation from DJ-1 to PTEN to facilitate keloid formation via the PI3K/AKT/mTOR pathway. Briefly, PTEN, as a negative regulating factor for the PI3K/AKT signaling pathway, acts as a brake on this pathway in normal skin. However, a higher SNO-DJ-1 level exists in keloids, which increases the level of PTEN S-nitrosylated at its Cys136 residue via transnitrosylation, thus diminishing the phosphatase activity of PTEN, activating the PI3K/AKT/mTOR pathway and promoting keloid formation. *DJ-1* parkinson disease protein 7, *PTEN* phosphatase and tensin homolog, *SNO* S-nitrosylation, *PI3K* phosphatidylinositol 3-kinase, *PIP2* phosphatidylinositol diphosphate, *PIP3* inositol triphosphate

to dysregulation of this and other pathways, resulting in overgrowth [37,38]. PTEN has also been shown to prevent dermal fibrotic lesions such as scleroderma and hypertrophic scarring, as well as renal and pulmonary fibrosis [39–42]. In our study, PTEN was identified via TurboID-based proximity labelling combined with LC–MS analysis as a potential target of DJ-1. We then verified that DJ-1 interacted with PTEN to induce SNO of the PTEN protein. The SNO-PTEN protein level was found to be higher in keloids, consistent with the higher SNO-DJ-1 level. Moreover, we identified Cys136 as the residue of the PTEN protein that underwent S-nitrosylation by MS analysis. Protein SNO mainly occurs in two ways: direct SNO of the sulfhydryl groups of cysteine residues and transnitrosylation [7]. Here, we found that the SNO of PTEN was the result of transnitrosylation from SNO-DJ-1. When we overexpressed the C106A mutant of DJ-1 in endogenous DJ-1-KO keloid fibroblasts, the SNO-PTEN level was notably reduced, even in the presence of SNOC, which could explain that exogenous treatment with the NO donor SNOC increased the level of SNO-PTEN by generating SNO-DJ-1 and increasing transnitrosylation, as shown in Figure 4c.

Dysregulation of the PI3K/AKT/mTOR signaling pathway is known to initiate the development of several diseases, including cancer and its progression, obesity, cardiovascular disease and diabetes [43–46]. It is also known that the PI3K/AKT/mTOR pathway plays an important role in the formation of keloids [47]. The phosphorylation of members of the PI3K/AKT pathway was reported to be enhanced by hypoxia, which might mediate metabolism in keloid fibroblasts [48]. Since PTEN is a negative regulator of this pathway, we demonstrated that PTEN protein SNO decreased the phosphatase activity of PTEN, thus mediating the activation effect of DJ-1 on the PI3K/AKT/mTOR pathway. When we knocked out DJ-1 in keloid fibroblasts, the PI3K/AKT/mTOR pathway was blocked, and activation of this pathway increased upon WT DJ-1 overexpression but not overexpression of the C106A mutant. Finally, we found that PI3K and AKT inhibitors could block the ability of DJ-1 to promote keloid fibroblast proliferation, migration and invasion, and collagen formation, demonstrating that DJ-1 promotes keloid formation in a manner dependent on the PI3K/AKT/mTOR pathway.

In view of the role of protein SNO in disease, a series of therapeutic measures targeting SNO are gradually proving feasible. For example, SNO-GNAI2 has been suggested as a therapeutic target against diabetes-accelerated atherosclerosis, and melatonin has been verified to have therapeutic effects by reducing SNO-GNAI2-induced deactivation of the Hippo–YAP axis [28]. Moreover, oral nitrite treatment was demonstrated to be important in the treatment of hypertension and other cardiovascular diseases that result from abnormal activation of the renin–angiotensin system because it can increase the generation of nitrosylating species and promote the nitrosylation of vascular proteins, including protein kinase C [49]. Given the findings of our study, it would be worthwhile to further develop drugs targeting SNO-DJ-1 to improve the clinical efficacy of keloid treatments (Figure 7).

Conclusions

DJ-1 is an essential positive modulator of keloid formation. A higher SNO-DJ-1 level was observed in keloids, and the ability of DJ-1 to promote proliferation, migration and

invasion as well as collagen generation in keloid fibroblasts is dependent on SNO of the Cys106 residue of the DJ-1 protein. SNO-DJ-1 increased the level of PTEN S-nitrosylated at its Cys136 residue via transnitrosylation in keloids, thus diminishing the phosphatase activity of PTEN and activating the PI3K/AKT/mTOR pathway. Importantly, the biological effect of DJ-1 in keloids is dependent on the SNO-DJ-1/SNO-PTEN/PI3K/AKT/mTOR axis. These findings may provide important new perspectives for keloid treatment.

Funding

We thank Shanghai Applied Protein Technology Co., Ltd. for assistance with the liquid chromatography-mass spectrometry analysis. This study was supported by grants from the National Natural Science Foundation of China (No. 82272273, No. 82072181, No. 81871565, No. 81571908) and the Sun Yat-sen University Clinical Research 5010 Program (No. 2018003).

Authors' contributions

BT, WD and XC conceived of, designed and supervised the study; DL, ZH and PC performed the experiments and analyzed the data; YD, ZX, YR, HX and ZW provided technical assistance with the experiments; and DL wrote the manuscript. All co-authors have reviewed and approved this version of the manuscript.

Conflicts of interest

None declared.

References

1. Jagdeo J, Kerby E, Glass DA, 2nd. Keloids. *JAMA Dermatol*. 2021;157:744.
2. Limandjaja GC, Niessen FB, Scheper RJ, Gibbs S. The keloid disorder: heterogeneity, histopathology, mechanisms and models. *Front Cell Dev Biol*. 2020;8:360.
3. Hawash AA, Ingrasci G, Nouri K, Yosipovitch G. Pruritus in keloid scars: mechanisms and treatments. *Acta Derm Venereol*. 2021;101:adv00582.
4. Li Y, Li M, Qu C, Li Y, Tang Z, Zhou Z, *et al*. The polygenic map of keloid fibroblasts reveals fibrosis-associated gene alterations in inflammation and immune responses. *Front Immunol*. 2021;12:810290.
5. Grabowski G, Pacana MJ, Chen E. Keloid and hypertrophic scar formation, prevention, and management: standard review of abnormal scarring in orthopaedic surgery. *J Am Acad Orthop Surg*. 2020;28:e408–14.
6. Gusarov I, Nudler E. Protein S-Nitrosylation: enzymatically controlled, but intrinsically unstable, Post-translational modification. *Mol Cell*. 2018;69:351–3.
7. Fernando V, Zheng X, Walia Y, Sharma V, Letson J, Furuta S. S-Nitrosylation: An emerging paradigm of redox Signaling. *Antioxidants (Basel)*. 2019;8:404.
8. Zhao Q, Ma J, Xie F, Wang Y, Zhang Y, Li H, *et al*. Recent advances in predicting protein S-Nitrosylation sites. *Biomed Res Int*. 2021;2021:5542224.
9. Sharma V, Fernando V, Letson J, Walia Y, Zheng X, Fackelman D, *et al*. S-Nitrosylation in tumor microenvironment. *Int J Mol Sci*. 2021;22:4600. https://doi.org/10.3390/ijms22094600.
10. Zhou HL, Premont RT, Stamler JS. The manifold roles of protein S-nitrosylation in the life of insulin. *Nat Rev Endocrinol*. 2022;18:111–28.
11. Nakamura T, Oh CK, Zhang X, Tannenbaum SR, Lipton SA. Protein Transnitrosylation Signaling networks contribute to Inflammaging and neurodegenerative disorders. *Antioxid Redox Signal*. 2021;35:531–50.
12. Dasgupta S, Gomez JJ, Singh I, Khan M. S-Nitrosylation in regulation of inflammation and cell damage. *Curr Drug Targets*. 2018;19:1831–8.
13. Malone-Povolny MJ, Maloney SE, Schoenfisch MH. Nitric oxide therapy for diabetic wound healing. *Adv Healthc Mater*. 2019;8:e1801210.
14. Neves M, Graos M, Anjo SI, Manadas B. Modulation of signaling pathways by DJ-1: An updated overview. *Redox Biol*. 2022;51:102283.
15. Nagakubo D, Taira T, Kitaura H, Ikeda M, Tamai K, Iguchi-Ariga SM, *et al*. DJ-1, a novel oncogene which transforms mouse NIH3T3 cells in cooperation with ras. *Biochem Biophys Res Commun*. 1997;231:509–13.
16. Huang M, Chen S. DJ-1 in neurodegenerative diseases: pathogenesis and clinical application. *Prog Neurobiol*. 2021;204:102114.
17. Xu M, Wu H, Li M, Wen Y, Yu C, Xia L, *et al*. DJ-1 deficiency protects hepatic steatosis by enhancing fatty acid oxidation in mice. *Int J Biol Sci*. 2018;14:1892–900.
18. De Lazzari F, Prag HA, Gruszczyk AV, Whitworth AJ, Bisaglia M. DJ-1: a promising therapeutic candidate for ischemia-reperfusion injury. *Redox Biol*. 2021;41:101884.
19. Lev N, Barhum Y, Lotan I, Steiner I, Offen D. DJ-1 knockout augments disease severity and shortens survival in a mouse model of ALS. *PLoS One*. 2015;10:e0117190.
20. Kim HS, Nam ST, Mun SH, Lee SK, Kim HW, Park YH, *et al*. DJ-1 controls bone homeostasis through the regulation of osteoclast differentiation. *Nat Commun*. 2017;8:1519.
21. Dong Y, Lv D, Zhao Z, Xu Z, Hu Z, Tang B. Lycorine inhibits hypertrophic scar formation by inducing ROS-mediated apoptosis. *Front Bioeng Biotechnol*. 2022;10:892015.
22. Lv D, Ding S, Zhong L, Tu J, Li H, Yao H, *et al*. M(6)a demethylase FTO-mediated downregulation of DACT1 mRNA stability promotes Wnt signaling to facilitate osteosarcoma progression. *Oncogene*. 2022;41:1727–41.
23. Ding S, Wang X, Lv D, Tao Y, Liu S, Chen C, *et al*. EBF3 reactivation by inhibiting the EGR1/EZH2/HDAC9 complex promotes metastasis via transcriptionally enhancing vimentin in nasopharyngeal carcinoma. *Cancer Lett*. 2022;527:49–65.
24. Hao G, Derakhshan B, Shi L, Campagne F, Gross SS. SNOSID, a proteomic method for identification of cysteine S-nitrosylation sites in complex protein mixtures. *Proc Natl Acad Sci U S A*. 2006;103:1012–7.
25. Kwak YD, Ma T, Diao S, Zhang X, Chen Y, Hsu J, *et al*. NO signaling and S-nitrosylation regulate PTEN inhibition in neurodegeneration. *Mol Neurodegener*. 2010;5:49.

26. Bonifati V, Rizzu P, van Baren MJ, Schaap O, Breedveld GJ, Krieger E, *et al.* Mutations in the DJ-1 gene associated with autosomal recessive early-onset parkinsonism. *Science*. 2003;299:256–9.
27. Chen G, An N, Ye W, Huang S, Chen Y, Hu Z, *et al.* bFGF alleviates diabetes-associated endothelial impairment by down-regulating inflammation via S-nitrosylation pathway. *Redox Biol*. 2021;41:101904.
28. Chao ML, Luo S, Zhang C, Zhou X, Zhou M, Wang J, *et al.* S-nitrosylation-mediated coupling of G-protein alpha-2 with CXCR5 induces hippo/YAP-dependent diabetes-accelerated atherosclerosis. *Nat Commun*. 2021;12:4452.
29. Branon TC, Bosch JA, Sanchez AD, Udeshi ND, Svinkina T, Carr SA, *et al.* Efficient proximity labeling in living cells and organisms with TurboID. *Nat Biotechnol*. 2018;36:880–7.
30. Cho KF, Branon TC, Udeshi ND, Myers SA, Carr SA, Ting AY. Proximity labeling in mammalian cells with TurboID and split-TurboID. *Nat Protoc*. 2020;15:3971–99.
31. Hsieh SC, Lai CS, Chang CH, Yen JH, Huang SW, Feng CH, *et al.* Nitric oxide: is it the culprit for the continued expansion of keloids? *Eur J Pharmacol*. 2019;854:282–8.
32. Hsu YC, Wang LF, Chien YW, Lee WR. Induction of TIMP-1 and HSP47 synthesis in primary keloid fibroblasts by exogenous nitric oxide. *J Dermatol Sci*. 2007;45:37–44.
33. Hsu YC, Hsiao M, Wang LF, Chien YW, Lee WR. Nitric oxide produced by iNOS is associated with collagen synthesis in keloid scar formation. *Nitric Oxide*. 2006;14:327–34.
34. Kim KR, Cho EJ, Eom JW, Oh SS, Nakamura T, Oh CK, *et al.* S-Nitrosylation of cathepsin B affects autophagic flux and accumulation of protein aggregates in neurodegenerative disorders. *Cell Death Differ*. 2022;29:2137–50.
35. Zhao Q, Zheng K, Ma C, Li J, Zhuo L, Huang W, *et al.* PTPS facilitates compartmentalized LTBP1 S-Nitrosylation and promotes tumor growth under hypoxia. *Mol Cell*. 2020;77:95–107.e5.
36. Zhang L, Wang J, Wang J, Yang B, He Q, Weng Q. Role of DJ-1 in immune and inflammatory diseases. *Front Immunol*. 2020;11:994.
37. Post KL, Belmadani M, Ganguly P, Meili F, Dingwall R, McDiarmid TA, *et al.* Multi-model functionalization of disease-associated PTEN missense mutations identifies multiple molecular mechanisms underlying protein dysfunction. *Nat Commun*. 2020;11:2073.
38. Yehia L, Keel E, Eng C. The clinical Spectrum of PTEN mutations. *Annu Rev Med*. 2020;71:103–16.
39. Parapuram SK, Shi-wen X, Elliott C, Welch ID, Jones H, Baron M, *et al.* Loss of PTEN expression by dermal fibroblasts causes skin fibrosis. *J Invest Dermatol*. 2011;131:1996–2003.
40. Guo L, Chen L, Bi S, Chai L, Wang Z, Cao C, *et al.* PTEN inhibits proliferation and functions of hypertrophic scar fibroblasts. *Mol Cell Biochem*. 2012;361:161–8.
41. Yu C, Xiong C, Tang J, Hou X, Liu N, Bayliss G, *et al.* Histone demethylase JMJD3 protects against renal fibrosis by suppressing TGFbeta and notch signaling and preserving PTEN expression. *Theranostics*. 2021;11:2706–21.
42. Parapuram SK, Thompson K, Tsang M, Hutchenreuther J, Bekking C, Liu S, *et al.* Loss of PTEN expression by mouse fibroblasts results in lung fibrosis through a CCN2-dependent mechanism. *Matrix Biol*. 2015;43:35–41.
43. Nunnery SE, Mayer IA. Targeting the PI3K/AKT/mTOR pathway in hormone-positive breast cancer. *Drugs*. 2020;80:1685–97.
44. Xie X, Man X, Zhu Z, Yuan D, Huang S. Tumor suppressor RIZ1 in obesity and the PI3K/AKT/mTOR pathway. *Obesity (Silver Spring)*. 2016;24:389–97.
45. Pi S, Mao L, Chen J, Shi H, Liu Y, Guo X, *et al.* The P2RY12 receptor promotes VSMC-derived foam cell formation by inhibiting autophagy in advanced atherosclerosis. *Autophagy*. 2021;17:980–1000.
46. Bathina S, Gundala NKV, Rhenghachar P, Polavarapu S, Hari AD, Sadananda M, *et al.* Resolvin D1 ameliorates nicotinamide-streptozotocin-induced type 2 diabetes mellitus by its anti-inflammatory action and modulating PI3K/Akt/mTOR pathway in the brain. *Arch Med Res*. 2020;51:492–503.
47. Xin Y, Min P, Xu H, Zhang Z, Zhang Y, Zhang Y. CD26 upregulates proliferation and invasion in keloid fibroblasts through an IGF-1-induced PI3K/AKT/mTOR pathway. *Burns Trauma*. 2020;8:tkaa025.
48. Wang Q, Wang P, Qin Z, Yang X, Pan B, Nie F, *et al.* Altered glucose metabolism and cell function in keloid fibroblasts under hypoxia. *Redox Biol*. 2021;38:101815.
49. Pinheiro LC, Oliveira-Paula GH, Ferreira GC, Dal-Cin de Paula T, Duarte DA, Costa-Neto CM, *et al.* Oral nitrite treatment increases S-nitrosylation of vascular protein kinase C and attenuates the responses to angiotensin II. *Redox Biol*. 2021;38:101769.